

# Origin of insulating state in bulk 1T-TaS<sub>2</sub> revealed by out-of-plane dimerization

Achyut Tiwari, Maxim Wenzel, Renjith Mathew Roy, Christian Prange, Bruno Gompf, and Martin Dressel  
 1. *Physikalisches Institut, Universität Stuttgart Pfaffenwaldring 57, 70569 Stuttgart, Germany*

The commensurate charge-density-wave phase in the prototypical transition metal dichalcogenide 1T-TaS<sub>2</sub> is investigated by temperature and polarization-dependent infrared spectroscopy revealing the fundamentally different charge dynamics parallel and perpendicular to the layers. Supported by density-functional-theory calculations, we demonstrate that the out-of-plane response is governed by a quasi-one-dimensional, Peierls-like dimerization of the two-dimensional star-of-David layers. In particular, our results identifies this dimerization as the primary driving mechanism of the metal-to-insulator transition, ruling out a significant role of electronic correlations.

Layered quantum materials provide a natural platform to study collective electronic phases, where the ground state is set not only by the properties of individual atomic layer but also by interlayer coupling through van der Waals interaction, Coulomb interactions, hybridization, and charge transfer [1–3]. Transition-metal dichalcogenides (TMDs) are a widely studied family in this class, hosting correlated and symmetry-broken phases, and their interlayer degree of freedom can now be tuned by twist, pressure, and designed heterostructures to access regimes such as moiré-driven superconductivity and engineered heavy-fermion behavior [4, 5].

1T-TaS<sub>2</sub> is a prototypical TMD characterized by a sequence of charge-density-wave (CDW) phases and pressure-induced superconductivity [6–8]. Upon cooling, it undergoes a sequence of transitions: from an incommensurate to a nearly commensurate metallic CDW phase (NCCDW), and then enters an insulating commensurate CDW (CCDW) phase below  $\sim 190$  K. This transition is first order, exhibits hysteresis, and progresses through an intermediate triclinic state upon warming [9, 10]. In the commensurate phase, a  $\sqrt{13} \times \sqrt{13}$  lattice distortion forms Star-of-David clusters, creating a narrow, half-filled band near the Fermi level. In the absence of interlayer coupling, suppressed intralayer hopping renders the system a Mott insulator, with localized  $S = 1/2$  spins on the triangular lattice of central Ta atoms, making 1T-TaS<sub>2</sub> a compelling candidate for realizing a quantum spin liquid ground state [11–13].

While the low-temperature insulating state in 1T-TaS<sub>2</sub> was originally attributed to purely two-dimensional electronic correlations and described as a Mott insulator [14, 15], emerging theoretical and experimental evidence has challenged this picture. Recent theoretical calculations suggest that interlayer coupling plays a significant role in shaping the in-plane electronic structure, and opening an insulating gap even without invoking strong on-site Coulomb interactions [16–18]. Recently, energy dependent angle-resolved photoemission spectroscopy (ARPES) study have reported finite dispersion along the out-to-plane direction [19]. At the same time, scanning tunneling microscopy (STM) shows that the local spectrum depends strongly on termination and stacking, and advanced many-body theory suggests that correlation effects can coexist with a stacking-driven hy-

bridization gap, especially near surfaces or locally perturbed regions [20–22].

Despite these advances, the bulk electronic response perpendicular to the planes direction remains poorly understood. ARPES and STM are intrinsically surface-sensitive and therefore do not directly access the electrodynamics across many stacked layers. Recent transport measurements on 1T-TaS<sub>2</sub> have revealed an unconventional resistivity anisotropy, with in-plane conduction more suppressed than out-of-plane, in stark contrast to the usual behavior of quasi-two-dimensional materials [23]. This highlights the need to clarify charge dynamics perpendicular to the layers, in order to resolve the true nature of the low-temperature ground state of 1T-TaS<sub>2</sub> and to advance the design of functional layered quantum materials. In particular, direct probes of the out-of-plane electronic response are essential for disentangling the intertwined effects of stacking order, dimerization, and electronic reconstruction, and for establishing how interlayer interactions govern the phase transitions in these systems.

In this letter, we report the optical spectroscopic measurements to access the electrodynamics of 1T-TaS<sub>2</sub> along the out-of-plane direction. Fourier-transform infrared measurements stands out as a highly effective technique for examining band modifications, probing a broad range of energies below, as well as above the Fermi level. We find that the CCDW transition produces a clear  $c$ -axis gap and a stacking-dependent redistribution of optical spectral weight. Corroborated by density-functional-theory (DFT) calculations, our findings reveal a Peierls-like interlayer dimerization that drives three-dimensional electronic reconstruction across the CCDW phase. Importantly, we demonstrate that the metal-insulator transition is governed by this stacking-induced dimerization rather than a correlation-driven Mott localization.

High-quality single crystals of 1T-TaS<sub>2</sub> (HQ Graphene Co.) were grown by chemical vapor transport (CVT) and characterized using dc-resistivity measurements. Temperature-dependent (10 - 300 K) and polarization-resolved infrared reflectivity was measured on an ion-beam-polished, optically flat crystal surfaces, shown in the inset of Fig.1, over a broad frequency range (200 – 18000 cm<sup>-1</sup>). The optical conductivity was obtained via Kramers–Kronig analysis, with full experimental details

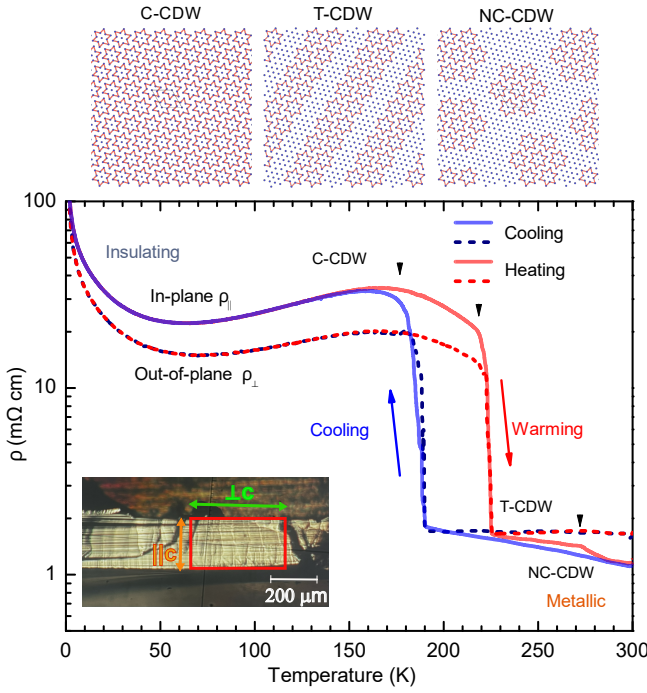


FIG. 1. Temperature-dependent resistivity of a 1T-TaS<sub>2</sub> single crystal upon cooling and heating. Black arrows mark the CDW phase transitions. Schematic illustrations (top) depict the sequence of nearly commensurate (NCCDW), triclinic (TCDW), and commensurate (CCDW) phases with decreasing temperature. The inset shows the ion-beam-polished cross-section of 1T-TaS<sub>2</sub> single crystal used for the polarization-resolved infrared spectroscopy with green and orange arrows indicating the polarization along and perpendicular to *c*-axis.

provided in the Supplemental Material [24].

Figure 1(b) displays the temperature dependence of the in-plane ( $\rho_{\parallel}$ ) and out-of-plane ( $\rho_{\perp}$ ) resistivities of 1T-TaS<sub>2</sub>. Consistent with previous studies,  $\rho_{\parallel}$  exhibits a nearly commensurate (NC) to commensurate (C) CDW transition, accompanied by a first-order metal-insulator transition at  $T_{CCDW} \approx 190$  K upon cooling, and a broad thermal hysteresis with an intermediate triclinic phase upon heating. Notably,  $\rho_{\perp}$  follows a similar temperature evolution but with unexpectedly low anisotropy. Intriguingly, in the NC-CDW phase,  $\rho_{\parallel}$  increases upon cooling, whereas  $\rho_{\perp}$  decreases, displaying a more conventional metallic behavior. This counterintuitive trend indicates that nanoscale domains in the NC-CDW phase strongly suppress in-plane conduction, whereas interlayer hopping dominates the charge transport.

The temperature-dependent optical conductivity, with the incident electric field polarized perpendicular and parallel to the *c*-axis is presented in Fig. 2(a) and (b), respectively. The in-plane ( $\perp c$ ) optical response agrees well with the earlier reports [25, 26], corroborating the robustness of our measurements. In the NC-CDW phase, both in-plane and out-of-plane optical conductivities ex-

hibit a weak Drude-like response below  $\omega < 1000$  cm<sup>-1</sup>. Interestingly, for the in-plane direction, the low-energy spectral weight decreases upon cooling [see inset of Fig. 2 (c)], resembling thermally activated behavior. In contrast, for the out-of-plane direction, the low-energy spectral weight increases [see inset of Fig. 2 (d)], reflecting the more conventional metallic behavior observed in the dc resistivity.

Upon cooling below  $T_{CCDW}$ , the optical conductivities show a pronounced suppression below  $\sim 1000$  cm<sup>-1</sup>, consistent with a gap opening, resulting in insulating behavior. In the in-plane direction, this is additionally accompanied by a notable appearance of phonons at lower frequencies, as electronic screening is reduced. Apart from the expected sharpening of features upon cooling, the high-energy optical conductivity ( $\omega > 6000$  cm<sup>-1</sup>) remains largely unaffected by the phase transition along both directions. In contrast, the optical conductivities undergo significant changes in the mid-infrared range ( $1000$  cm<sup>-1</sup>  $< \omega < 6000$  cm<sup>-1</sup>), further indicating the three-dimensional character of the CCDW transition and the subsequent reconstruction of the electronic structure.

To gain further insight into the C-CDW transition-induced changes in the optical spectra, the optical conductivities are decomposed into a low-energy Drude response (purple), mid-infrared interband absorptions (orange), and high-energy interband absorptions (blue) [Figs. 2(c-f)]. Decomposed conductivity reveals a substantial redistribution of spectral weight from mid-infrared to higher-energy upon entering the C-CDW state, for both in-plane and out-of-plane direction. The suppressed spectral weight at low energies is recovered in the mid-infrared range ( $1000$  cm<sup>-1</sup>  $< \omega < 6000$  cm<sup>-1</sup>), signaling a pronounced reconstruction of the electronic band structure that involves not only states within the CDW planes but also interlayer electronic coupling. The gap energy,  $2\Delta_{CDW}$ , can be obtained by extrapolating the steepest part of the absorption edge to zero, as illustrated by the dashed lines in Fig. 2(a) and (b), yielding the values  $\sim 135$  meV and  $\sim 150$  meV at low temperature for in-plane and out-of-plane, respectively. Alternatively, the zero crossing of the difference optical conductivity  $\Delta\sigma_1 = \sigma_1^{\text{inter}}(\omega, T < T_{CDW}) - \sigma_1^{\text{inter}}(\omega, T > T_{CDW})$ , led to very similar values of  $2\Delta_{CDW}$  and their temperature difference normalized to 10 K. These  $2\Delta_{CDW}$  values are consistent with the previous infrared spectroscopy, ARPES and STM studies in the low-temperature phase, where apparent CDW and correlation related gaps range from 80 - 450 meV depending on surface termination, stacking, and correlation strength [19, 22, 25]. Moreover,  $2\Delta_{CDW} \approx 150$  meV in out-of-plane direction is consistent with the  $k_z$  bandwidth of the narrow band (about 140 meV from photon-energy dependent ARPES), underscoring that the perpendicular gap is constrained by interlayer dispersion rather than solely by in-plane CDW reconstruction [19].

Inset of Fig. 2(b) displays the temperature evolution of the CDW gap. Remarkably, the in-plane gap exhibits

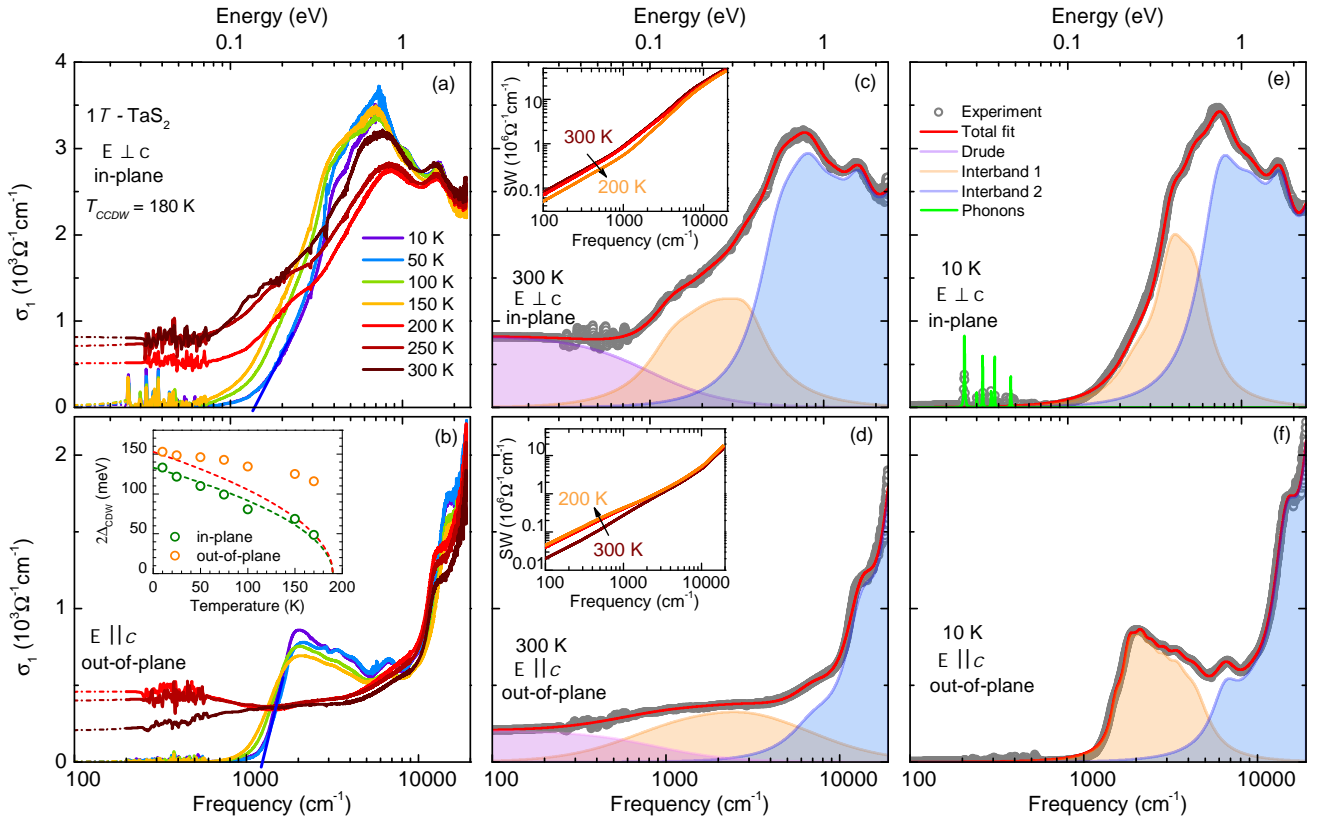


FIG. 2. **Temperature-dependent optical conductivity of 1T-TaS<sub>2</sub>.** (a, b) Real part of the optical conductivity  $\sigma_1(\omega)$  of 1T-TaS<sub>2</sub> along the in-plane (*ab*-plane) and out-of-plane (*c*-axis) directions, calculated from the measured reflectivity via Kramers-Kronig analysis. (c–f) Decomposition of the optical conductivity into Drude (purple), low energy (LE) interband transitions (orange), and high-energy (HE) interband transitions (blue) and phonon modes (green) for the in-plane (c, e), out-of-plane (d, f) directions at  $T = 300$  K and  $T = 10$  K, respectively. The extrapolation of the steepest part to the frequency axis is taken as the  $2\Delta_{\text{CDW}}$ . The inset (b) shows the temperature evolution of the gap obtained from the extrapolation of the absorption edge for in-plane and out-of-plane and the insets (c,d) show the frequency-dependent spectral weight (SW) in the NC-CDW phase.

a mean-field-like temperature dependence, which can be described by  $\Delta(T) \approx \Delta(0 \text{ K}) \sqrt{1 - \frac{T}{T_{\text{CDW}}}}$ , where we assume  $T_{\text{CDW}} = 190$  K and  $\Delta(0 \text{ K}) = 135$  meV. In contrast, the out-of-plane gap evolves more abruptly and cannot be captured by the mean-field formula, suggesting a fundamentally different nature of the metal-to-insulator transition along this direction. Notably, a similar deviation from mean-field behavior has been reported in kagome metals with star-of-David-type in-plane lattice modulations. However, in those systems, the deviation appears in the in-plane gap [27].

The combined transport and optical responses demonstrate that the insulating ground state of 1T-TaS<sub>2</sub> is intrinsically three-dimensional instead of confining in 2D layers, with an energy gap opening along both the in-plane and out-of-plane directions. To further uncover the origin of this gap and its dependence on stacking geometry, we carried out DFT calculations of the electronic structure and optical conductivity for different CDW stacking configurations. Among various stacking orders,

the alternating-ladder (AL) stacking of dimerized bilayers shows good agreement with the experimental optical spectra as presented in Fig. 3. The calculated optical conductivity for the AL stacking not only captures the features of both in-plane and out-of-plane spectra but also yields energy gap scale in quantitative agreement with experiment [Fig. 3(c)]. Correspondingly, the band structure for the AL configuration shows a full gap opening at the Fermi level, consistent with our transport and optical results.

In contrast, other stacking arrangements fail to account for the experimental observed gap opening. Even when including on-site Coulomb interactions ( $U$ ), other stacking orders do not exhibit a complete gap at the Fermi level, nor do their optical conductivities reproduce the observed spectral weight redistribution [see Fig.S3 and S4 in Supplemental Material [24]]. This strongly indicates that the insulating ground state of bulk 1T-TaS<sub>2</sub> originates from stacking-selective dimerization of CDW bilayers, which couples the layers into a coherent three-dimensional band-insulating phase.

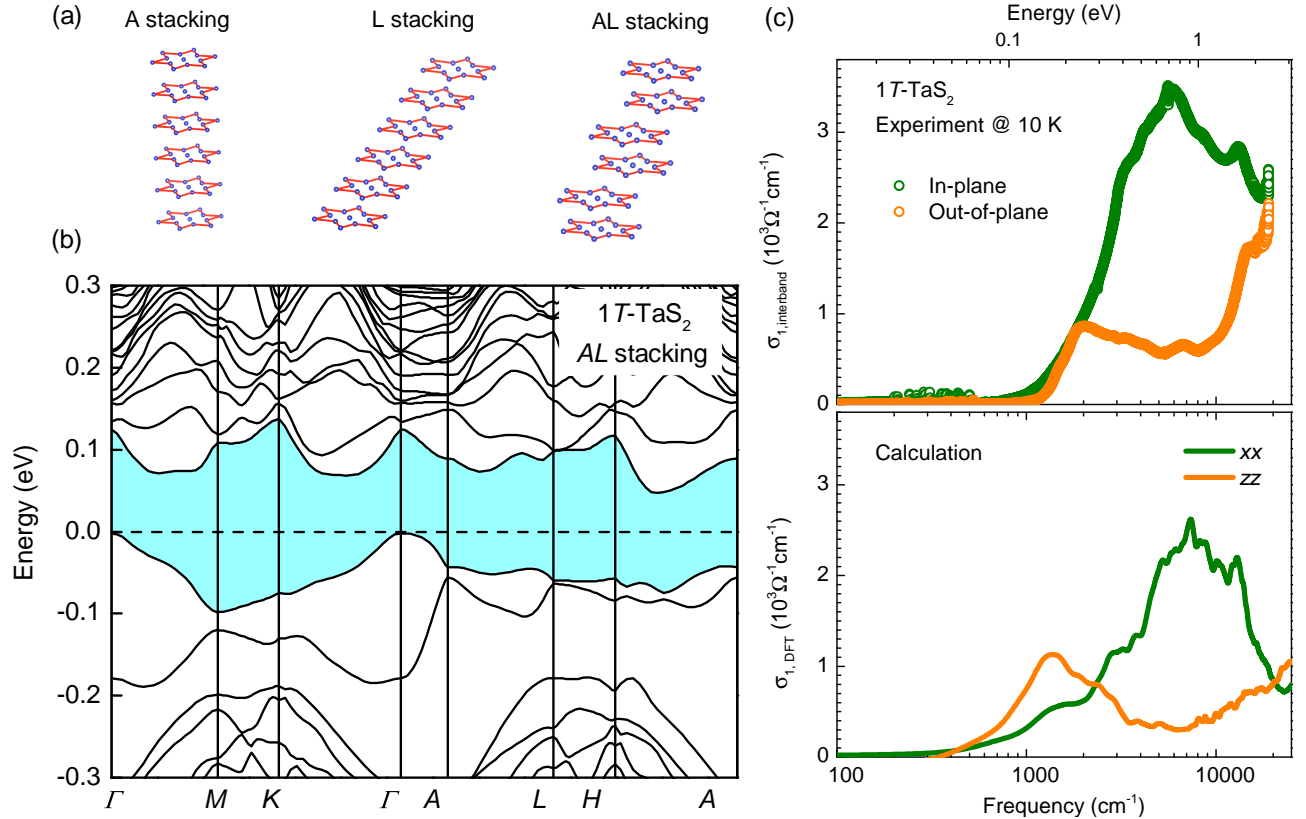


FIG. 3. (a) Schematic A, L, and AL stacking of star-of-David cluster along out-of-plane directions. (b) Calculated band structure for the low-temperature CCDW phase for AL stacking with the shaded region highlights the gap at the Fermi level. (c) Comparison of the measured real part of the optical conductivity,  $\sigma_1(\omega)$ , with the optical response calculated from density-functional theory for the AL-stacked commensurate CDW structure.

Our results are consistent with recent theoretical investigations [16, 17] and  $k_z$ -resolved ARPES measurements[19], which demonstrate that the electronic gap in bulk 1T-TaS<sub>2</sub> crucially depends upon the interlayer stacking configuration. From our recent ellipsometry study [28] that concluded the transition is inherently three-dimensional, highlighting the pivotal role of interlayer coupling in phase evolution. Here, a comparative analysis of calculated optical conductivities for different stacking-geometries with and experimental spectra demonstrates that the gap-opening mechanism is extremely sensitive to the out-of-plane stacking ordering [18]. Furthermore, while our findings do not exclude the presence of electron-electron interactions, they strongly suggest that the primary driver of the phase transition is Peierls-like interlayer dimerization of Star-of-David layers that doubles the periodicity along  $c$ -axis, as proposed by X-ray diffraction studies [20, 29, 30]. These observations indicate that the bulk ground state is a three-dimensional band insulator, thereby challenging the Mott insulating picture in bulk and, consequently, the realization of quantum spin liquid (QSL) phase [11, 12]. Nevertheless, the extreme stacking sensitivity, as indicated by both theoretical and experimental findings, suggests

a tangible approach to materials manipulation: stacking faults, interlayer sliding, and optically or electrically induced restacking can selectively modulate interlayer hybridization, thereby altering the electronic gap. This provides a foundation for engineering domain-wall metallicity, nonequilibrium phases, and flat-band regimes in specifically designed TaS<sub>2</sub> heterostructures [31–34].

In conclusion, optical spectroscopy combined with DFT calculations clarify the out-of-plane charge dynamics of 1T-TaS<sub>2</sub> across the first-order CCDW transition. The anomalous dc anisotropy in the NCCDW phase evidences enhanced interlayer hopping, deviating from the conventional quasi-two-dimensional behaviour. The low-temperature optical response reveals a spontaneous gap opening in the out-of-plane direction, distinct from the in-plane gap scale, and the observed spectral-weight transfer and gap formation are reproduced only for stacking configurations that realize interlayer dimerization. These results identify a quasi-one-dimensional, Peierls-like instability along the  $c$  axis as the key ingredient stabilizing the bulk insulating state, and they establish interlayer stacking as an essential control parameter of the metal-insulator transition in 1T-TaS<sub>2</sub>, motivating targeted stacking engineering to tune correlated and

nonequilibrium phases in layered CDW materials.

**Acknowledgments:** We thank Gabriele Untereiner (Universität Stuttgart) and Bernhard Fenk (Nanostructuring Lab, Max Planck Institute for Solid State Research, Stuttgart) for technical support. We also thank Prof. Liang Cao (Chinese Academy of Sciences, Hefei,

China) and Dr. Tobias Ritschel (Technische Universität Dresden) for providing atomic structures for the different stacking configurations. This work at Universität Stuttgart is supported by the Deutsche Forschungsgemeinschaft (DFG) under Grant No. DR228/63-1 and GO642/8-1.

---

[1] K. S. Novoselov, D. Jiang, F. Schedin, T. Booth, V. Khotkevich, S. Morozov, and A. K. Geim, Two-dimensional atomic crystals, *Proc. Natl Acad. Sci.* **102**, 10451 (2005).

[2] A. K. Geim and I. V. Grigorieva, Van der waals heterostructures, *Nature* **499**, 419 (2013).

[3] R. Mathew Roy, X. Feng, M. Wenzel, V. Hasse, C. Shekhar, M. G. Vergniory, C. Felser, A. V. Pronin, and M. Dressel, Interlayer Charge Transfer Induced by Electronic Instabilities in the Natural van der Waals Heterostructure  $4H_b$ -TaS<sub>2</sub>, *Phys. Rev. Lett.* **135**, 116503 (2025).

[4] Y. Cao, V. Fatemi, S. Fang, K. Watanabe, T. Taniguchi, E. Kaxiras, and P. Jarillo-Herrero, Unconventional superconductivity in magic-angle graphene superlattices, *Nature* **556**, 43 (2018).

[5] V. Vaňo, M. Amini, S. C. Ganguli, G. Chen, J. L. Lado, S. Kezilebieke, and P. Liljeroth, Artificial heavy fermions in a van der waals heterostructure, *Nature* **599**, 582 (2021).

[6] J. Wilson, F. D. Salvo, and S. Mahajan, Charge-density waves and superlattices in the metallic layered transition metal dichalcogenides, *Adv. Phys.* **24**, 117 (1975).

[7] E. Tosatti and P. Fazekas, On the nature of the low-temperature phase of 1T-TaS<sub>2</sub>, *J. Phys. Colloq.* **37**, C4 (1976).

[8] B. Sipos, A. F. Kusmartseva, A. Akrap, H. Berger, L. Forró, and E. Tutiš, From Mott state to superconductivity in 1T-TaS<sub>2</sub>, *Nat. mater.* **7**, 960 (2008).

[9] R. E. Thomson, B. Burk, A. Zettl, and J. Clarke, Scanning tunneling microscopy of the charge-density-wave structure in 1T-TaS<sub>2</sub>, *Phys. Rev. B* **49**, 16899 (1994).

[10] K. Rossnagel, On the origin of charge-density waves in select layered transition-metal dichalcogenides, *J. Phys. Condens. Matter* **23**, 213001 (2011).

[11] M. Kratochvílova, A. D. Hillier, A. R. Wildes, L. Wang, S.-W. Cheong, and J.-G. Park, The low-temperature highly correlated quantum phase in the charge-density-wave 1T-TaS<sub>2</sub> compound, *npj Quantum Mater.* **2**, 42 (2017).

[12] M. Klanjšek, A. Zorko, R. Žitko, J. Mravlje, Z. Jagličić, P. K. Biswas, P. Prelovšek, D. Mihailovic, and D. Arčon, A high-temperature quantum spin liquid with polaron spins, *Nat. Phys.* **13**, 1130 (2017).

[13] K. T. Law and P. A. Lee, 1T-TaS<sub>2</sub> as a quantum spin liquid, *Proc. Natl Acad. Sci. USA* **114**, 6996 (2017).

[14] P. Fazekas and E. Tosatti, Electrical, structural and magnetic properties of pure and doped 1T-TaS<sub>2</sub>, *Philos. Mag. B* **39**, 229 (1979).

[15] J.-J. Kim, W. Yamaguchi, T. Hasegawa, and K. Kitazawa, Observation of Mott Localization Gap Using Low Temperature Scanning Tunneling Spectroscopy in Commensurate 1T-TaS<sub>2</sub>, *Phys. Rev. Lett.* **73**, 2103 (1994).

[16] T. Ritschel, H. Berger, and J. Geck, Stacking-driven gap formation in layered 1T-TaS<sub>2</sub>, *Phys. Rev. B* **98**, 195134 (2018).

[17] S.-H. Lee, J. S. Goh, and D. Cho, Origin of the Insulating Phase and First-Order Metal-Insulator Transition in 1T-TaS<sub>2</sub>, *Phys. Rev. Lett.* **122**, 106404 (2019).

[18] T. Ritschel, J. Trinckauf, K. Koepernik, B. Büchner, M. v. Zimmermann, H. Berger, Y. Joe, P. Abbamonte, and J. Geck, Orbital textures and charge density waves in transition metal dichalcogenides, *Nat. phys.* **11**, 328 (2015).

[19] Y. D. Wang, W. L. Yao, Z. M. Xin, T. T. Han, Z. G. Wang, L. Chen, C. Cai, Y. Li, and Y. Zhang, Band insulator to Mott insulator transition in 1T-TaS<sub>2</sub>, *Nat. Commun.* **11**, 4215 (2020).

[20] F. Petocchi, C. W. Nicholson, B. Salzmann, D. Pasquier, O. V. Yazyev, C. Monney, and P. Werner, Mott versus Hybridization Gap in the Low-Temperature Phase of 1T-TaS<sub>2</sub>, *Phys. Rev. Lett.* **129**, 016402 (2022).

[21] S. H. Lee and D. Cho, Charge density wave surface reconstruction in a van der waals layered material, *Nat. Commun.* **14**, 5735 (2023).

[22] Y. Wang, Z. Li, X. Luo, J. Gao, Y. Han, J. Jiang, J. Tang, H. Ju, T. Li, R. Lv, S. Cui, Y. Yang, Y. Sun, J. Zhu, X. Gao, W. Lu, Z. Sun, H. Xu, Y. Xiong, and L. Cao, Dualistic insulator states in 1T-TaS<sub>2</sub> crystals, *Nat. Commun.* **15**, 3425 (2024).

[23] E. Martino, A. Pisoni, L. Čirić, A. Arakcheeva, H. Berger, A. Akrap, C. Putzke, P. J. Moll, I. Batistić, E. Tutiš, L. Forró, and K. Semeniuk, Preferential out-of-plane conduction and quasi-one-dimensional electronic states in layered 1T-TaS<sub>2</sub>, *npj 2D Mater. Appl.* **4**, 7 (2020).

[24] See Supplemental Material at [URL] for experimental details, data analysis, details on DFT calculations, and additional computational results, which includes Refs. [16, 22, 35–42].

[25] L. V. Gasparov, K. G. Brown, A. C. Wint, D. B. Tanner, H. Berger, G. Margaritondo, R. Gaál, and L. Forró, Phonon anomaly at the charge ordering transition in 1T-TaS<sub>2</sub>, *Phys. Rev. B* **66**, 094301 (2002).

[26] Z. Lin, J. Li, X. Cao, J. Gao, X. Luo, Y. Sun, Y. Lu, N. Wang, J. Guo, and X. Zhu, Interlayer hopping between a surface Mott insulator and a bulk band insulator in layered 1T-TaS<sub>2</sub>, *Phys. Rev. B* **111**, 075126 (2025).

[27] E. Uykur, B. R. Ortiz, O. Iakutkina, M. Wenzel, S. D. Wilson, M. Dressel, and A. A. Tsirlin, Low-energy optical properties of the nonmagnetic kagome metal CsV<sub>3</sub>Sb<sub>5</sub>, *Phys. Rev. B* **104**, 045130 (2021).

[28] A. Tiwari, B. Gompf, and M. Dressel, Interlayer coupling driven phase evolution in hyperbolic 1T-TaS<sub>2</sub>, *arXiv:2512.07508* (2025).

[29] S. Tanda, T. Sambongi, T. Tani, and S. Tanaka, X-Ray Study of Charge Density Wave Structure in 1T-TaS<sub>2</sub>, *J.*

Phys. Soc. Jpn. **53**, 476 (1984).

[30] C. Burri, H. G. Bell, F. Dizdarević, W. Hu, J. Ravnik, J. Vonka, Y. Ekinci, S.-W. Huang, S. Gerber, and N. Hua, Three-dimensional electronic domain correlations in 1T-TaS<sub>2</sub>, [arXiv:2508.17839](https://arxiv.org/abs/2508.17839) (2025).

[31] R. Hovden, A. W. Tsen, P. Liu, B. H. Savitzky, I. E. Baggari, Y. Liu, W. Lu, Y. Sun, P. Kim, A. N. Pasupathy, and L. F. Kourkoutis, Atomic lattice disorder in charge-density-wave phases of exfoliated dichalcogenides (1T-TaS<sub>2</sub>), Proc. Natl Acad. Sci. USA **113**, 11420 (2016).

[32] Q. Stahl, M. Kusch, F. Heinsch, G. Garbarino, N. Kretzschmar, K. Hanff, K. Rossnagel, J. Geck, and T. Ritschel, Collapse of layer dimerization in the photo-induced hidden state of 1T-TaS<sub>2</sub>, Nat. Commun. **11**, 1247 (2020).

[33] J. Liu, P. Liu, L. Yang, S.-H. Lee, M. Pan, F. Chen, J. Huang, B. Jiang, M. Hu, Y. Zhang, Z. Xie, G. Wang, M. Guan, W. Jiang, H. Yang, J. Li, C. Yun, Z. Wang, S. Meng, Y. Yao, T. Qian, and X. Shi, Nonvolatile optical control of interlayer stacking order in 1T-TaS<sub>2</sub>, npj Quantum Mater. [10.1038/s41535-025-00836-6](https://doi.org/10.1038/s41535-025-00836-6) (2025).

[34] H. Bae, R. Valentí, I. I. Mazin, and B. Yan, Designing flat bands, localized and itinerant states in TaS<sub>2</sub> trilayer heterostructures, npj Quantum Mater. **10**, 92 (2025).

[35] P. Giannozzi, S. Baroni, N. Bonini, M. Calandra, R. Car, C. Cavazzoni, D. Ceresoli, G. L. Chiarotti, M. Cococcioni, I. Dabo, A. Dal Corso, S. de Gironcoli, S. Fabris, G. Fratesi, R. Gebauer, U. Gerstmann, C. Gougaussis, A. Kokalj, M. Lazzeri, L. Martin-Samos, N. Marzari, F. Mauri, R. Mazzarello, S. Paolini, A. Pasquarello, L. Paulatto, C. Sbraccia, S. Scandolo, G. Sclauzero, A. P. Seitsonen, A. Smogunov, P. Umari, and R. M. Wentzcovitch, QUANTUM ESPRESSO: a modular and open-source software project for quantum simulations of materials, J. Phys. Condens. Matter **21**, 395502 (2009).

[36] P. Giannozzi, O. Andreussi, T. Brumme, O. Bunau, M. Buongiorno Nardelli, M. Calandra, R. Car, C. Cavazzoni, D. Ceresoli, M. Cococcioni, N. Colonna, I. Carnimeo, A. Dal Corso, S. de Gironcoli, P. Delugas, R. A. DiStasio, A. Ferretti, A. Floris, G. Fratesi, G. Fugallo, R. Gebauer, U. Gerstmann, F. Giustino, T. Gorni, J. Jia, M. Kawamura, H.-Y. Ko, A. Kokalj, E. Küçükbenli, M. Lazzeri, M. Marsili, N. Marzari, F. Mauri, N. L. Nguyen, H.-V. Nguyen, A. Otero-de-la Roza, L. Paulatto, S. Poncé, D. Rocca, R. Sabatini, B. Santra, M. Schlipf, A. P. Seitsonen, A. Smogunov, I. Timrov, T. Thonhauser, P. Umari, N. Vast, X. Wu, and S. Baroni, Advanced capabilities for materials modelling with Quantum ESPRESSO, J. Phys. Condens. Matter **29**, 465901 (2017).

[37] P. Blaha, K. Schwarz, G. Madsen, D. Kvasnicka, J. Luitz, R. Laskowski, F. Tran, and L. Marks, WIEN2k, An Augmented Plane Wave + Local Orbitals Program for Calculating Crystal Properties (Karlheinz Schwarz, Techn. Universität Wien, Austria), 2018. ISBN 3-9501031-1-2.

[38] P. Blaha, K. Schwarz, F. Tran, R. Laskowski, G. K. H. Madsen, and L. D. Marks, WIEN2k: An APW+lo program for calculating the properties of solids, J. Chem. Phys. **152**, 074101 (2020).

[39] V. Petkov, J. E. Peralta, B. Aoun, and Y. Ren, Atomic structure and Mott nature of the insulating charge density wave phase of 1T-TaS<sub>2</sub>, J. Phys. Condens. Matter **34**, 345401 (2022).

[40] C. Ambrosch-Draxl and J. O. Sofo, Linear optical properties of solids within the full-potential linearized augmented planewave method, Comput. Phys. Commun. **175**, 1 (2006).

[41] I.-H. Suh, Y.-S. Park, and J.-G. Kim, ORTHON: transformation from triclinic axes and atomic coordinates to orthonormal ones, J. Appl. Crystallogr. **33**, 994 (2000).

[42] K. Persson, Materials Data on TaS<sub>2</sub> (SG:164) by Materials Project (2014).

## Supplemental Material: Origin of insulating state in bulk 1T-TaS<sub>2</sub> revealed by out-of-plane dimerization

Achyut Tiwari, Maxim Wenzel, Renjith Mathew Roy, Christian Prange, Bruno Gompf, and Martin Dressel

1. *Physikalisches Institut, Universität Stuttgart, Pfaffenwaldring 57, 70569 Stuttgart, Germany*

(Dated: December 29, 2025)

### S1. CRYSTAL STRUCTURE AND PHASE TRANSITIONS

1T-TaS<sub>2</sub> is a quasi-two-dimensional material composed of S-Ta-S, stacked sequentially via weak van der Waals interactions. 1T-TaS<sub>2</sub> crystallize in the P3/m1 space group with trigonal symmetry in high-temperature undistorted phase. Each Ta atom is octahedrally coordinated by six sulfur (S) atoms, making a perfect hexagonal plane in this phase. Upon cooling, the system undergoes a sequence of phase transitions: from an incommensurate metallic CDW phase (IC-CDW) above 350 K, to a nearly commensurate metallic CDW phase (NC-CDW) between 180 K and 350 K, and finally to a commensurate insulating CDW phase (C-CDW) below 180 K, and a broad thermal hysteresis with an intermediate triclinic phase (T-CDW) upon heating. The CDW phase features a  $\sqrt{13} \times \sqrt{13}$  periodic lattice distortion (PLD), where the entire crystalline plane is tiled by Star of David (SD) clusters, making it commensurate with the atomic lattice. This superlattice is typically rotated by 13.9° with respect to the atomic lattice. Star of David (SD) Clusters: Consist of 13 Ta atoms. The 12 outer Ta atoms contract towards the central Ta atom. The displacement of Ta atoms is accompanied by bulging of the S layers.

### S2. EXPERIMENTAL DETAILS

High-quality single crystals of 1T-TaS<sub>2</sub> (HQ Graphene Co.) were grown by chemical vapor transport (CVT). Plate-like crystals with typical dimensions of  $5 \times 2 \text{ mm}^2$  and thickness  $\sim 200 \mu\text{m}$  were selected for transport and optical studies. Four-terminal resistivity was measured within the *ab* plane and along the *c* axis in a Physical Property Measurement System (PPMS, Quantum Design). For *c*-axis measurements, contacts were patterned on opposite faces to enforce uniaxial current flow and minimize geometric uncertainties.

To measure the *c*-axis optical response, the crystal cross-section was ion-beam polished (Leica cross-section polisher) to an optically flat surface (see inset of Fig.1 in main text). Infrared reflectivity at normal incidence was measured with a Bruker Vertex 80v spectrometer coupled to a Hyperion infrared microscope over 200–19,000,  $\text{cm}^{-1}$  (24.8 meV–2.35 eV) from 300 K down to 10 K. Polarization-resolved reflectivity was obtained with  $E \perp c$  (*ab*-plane response) and  $E \parallel c$ . Freshly evaporated gold mirror was used as reference for absolute reflectivity.

The complex optical conductivity was obtained from the measured reflectivity via Kramers–Kronig transformation. We applied Drude–Lorentz fits, utilizing the dc-conductivity obtained through transport measurements for extrapolations at lower frequencies, while x-ray scattering data were utilized to extrapolate the data in the high-frequency range.

S2

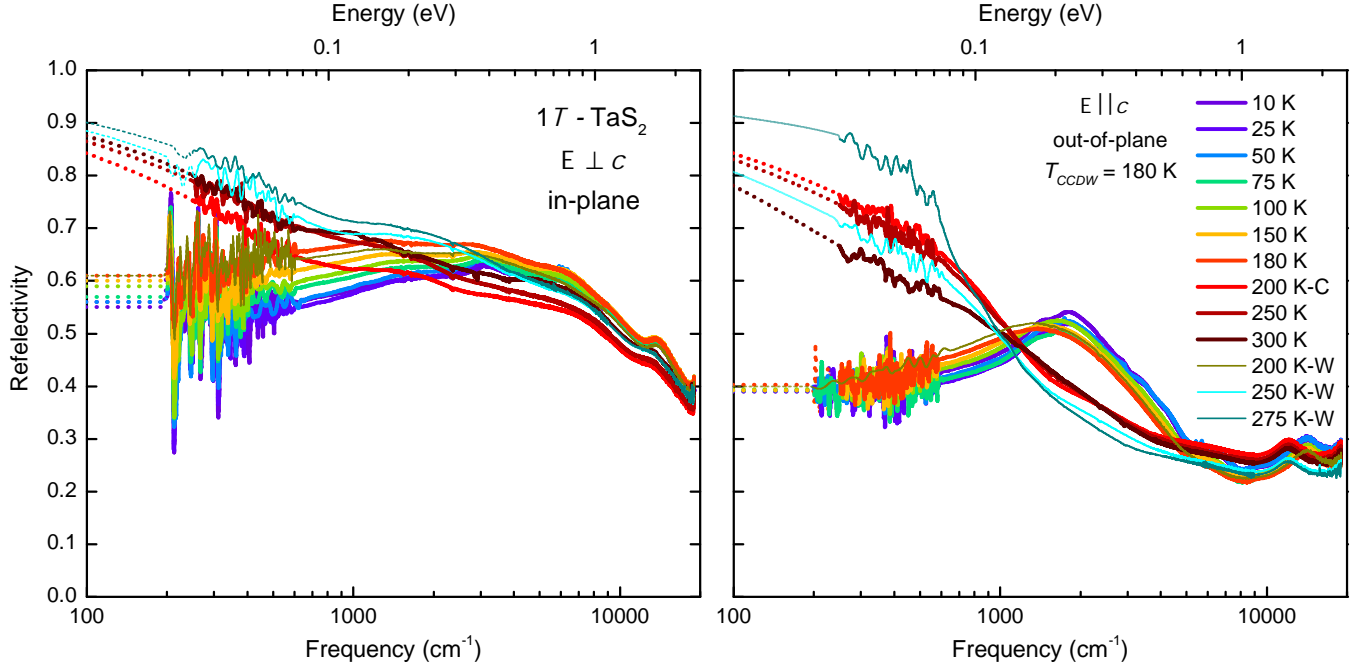


FIG. S1. Temperature-dependent reflectivity of a 1T-TaS<sub>2</sub> single crystal measured with light polarized perpendicular to the *c*-axis (*ab*-plane response, left) and parallel to the *c*-axis (right) over a broad spectral range. Upon cooling, the reflectivity along both directions exhibits a marked suppression in the low-frequency region, signaling the opening of an energy gap at the commensurate charge-density-wave (CCDW) transition. Dotted lines indicate low-energy extrapolations based on Drude–Lorentz modeling. Thin lines correspond to spectra measured upon heating, highlighting the pronounced thermal hysteresis associated with the first-order nature of the metal–insulator transition.

### S3. DECOMPOSITION OF OPTICAL SPECTRA

We modeled the optical spectra using a Drude–Lorentz approach, in which the total dielectric function is expressed as the sum of itinerant carriers (Drude contribution) and bound electronic excitations (Lorentz oscillators):

$$\tilde{\varepsilon}(\omega) = \varepsilon_{\infty} - \frac{\omega_{p,\text{Drude}}^2}{\omega^2 + i\omega/\tau_{\text{Drude}}} + \sum_j \frac{\Omega_j^2}{\omega_{0,j}^2 - \omega^2 - i\omega\gamma_j}. \quad (\text{S1})$$

where  $\varepsilon_{\infty}$  denotes the high-energy contribution,  $\omega_{p,\text{Drude}}$  and  $1/\tau_{\text{Drude}}$  are the plasma frequency and scattering rate of the itinerant carriers, and  $\omega_{0,j}$ ,  $\Omega_j$ , and  $\gamma_j$  are the resonance frequency, oscillator strength, and linewidth of the  $j^{\text{th}}$  excitation, respectively. The complex optical conductivity [ $\tilde{\sigma} = \sigma_1 + i\sigma_2$ ] is obtained from:

$$\tilde{\sigma}(\omega) = -i\omega[\tilde{\varepsilon} - \varepsilon_{\infty}]/4\pi. \quad (\text{S2})$$

The experimental optical spectra were fitted simultaneously to  $\varepsilon_1(\omega)$ ,  $\sigma_1(\omega)$ , and the reflectivity by varying these parameters. In addition to electronic contributions, sharp Lorentz oscillators were included to account for phonon modes, which become prominent in the insulating C-CDW phase for in-plane polarization. Representative decompositions of the optical conductivity are shown in Fig. 2 (main text) for  $T = 300$  K and 10 K, and in Fig. S2 for 200, 100, and 50 K.

In the NC-CDW phase, the in-plane ( $E \perp c$ ) Drude contribution weakens upon cooling, while the out-of-plane ( $E \parallel c$ ) Drude response strengthens, consistent with enhanced interlayer transport. Across  $T_{\text{CCDW}}$ , pronounced changes in the Lorentzian excitations and the emergence of sharp phonons in-plane highlight a redistribution of spectral weight and confirm that the electronic reconstruction is intrinsically three-dimensional.

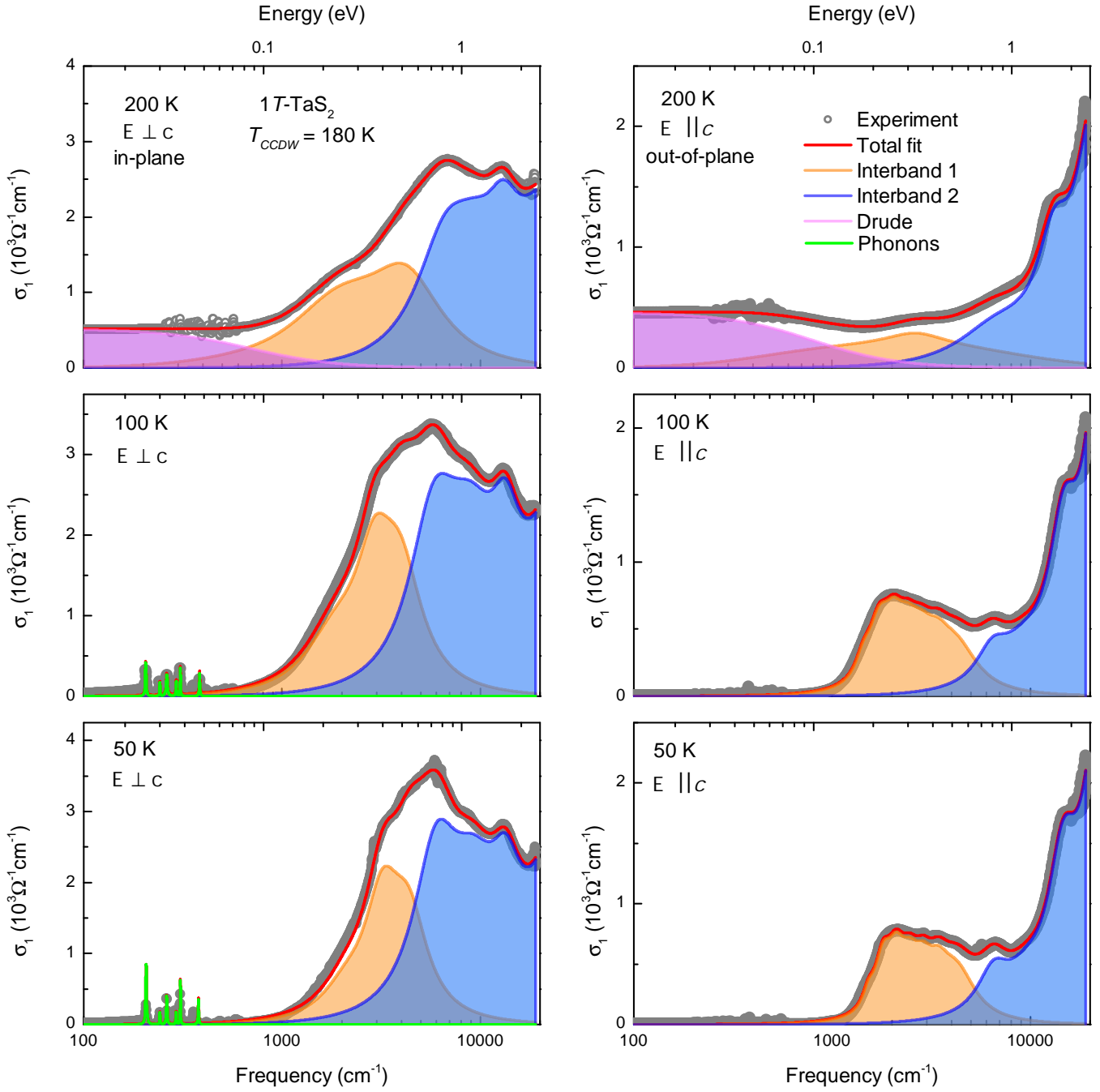


FIG. S2. Decomposition of the optical conductivity into a Drude component (magenta), mid-infrared interband transitions (orange), and high-energy interband transitions (blue) for the in-plane ( $E \perp c$ , left) and out-of-plane ( $E \parallel c$ , right) responses at 200 K, 100 K, and 50 K. The fits are obtained using the Drude–Lorentz approach, simultaneously fitting reflectivity,  $\sigma_1$ , and  $\varepsilon_1$ . Upon cooling, the in-plane Drude response weakens while the out-of-plane Drude response strengthens, highlighting the counterintuitive evolution of charge dynamics for layered materials. The pronounced redistribution of mid-infrared spectral weight in the low-temperature phase reflect a substantial reconstruction of the low-energy electronic structure across the CDW transition.

#### S4. DFT CALCULATIONS

Density-functional-theory calculations were performed in the **Quantum Espresso** and **Wien2k** codes [1–4] within the generalized gradient approximation (GGA) employing the Perdew-Burke-Ernzerhof exchange-correlation functional [5]. Spin-orbit coupling was included in all calculations. Self-consistent calculations of the CCDW phase with *AL* stacking [6], as presented in the main text, were converged on a  $4 \times 4 \times 4$   $k$ -mesh in **Quantum Espresso**, with the plane-wave energy cutoff and charge-density cutoff set to 30 Ry and 300 Ry, respectively. The optical conductivity was computed using the built-in `epsilon.x` module.

All other calculations presented in Section S5 were converged in **Wien2k** using the  $k$ -meshes summarized in Table S1. A Hubbard  $U_{\text{Ta}} = 2$  eV was added to the  $3d$  Ta orbitals of the CCDW crystal structure from Ref. [7], using the LDA+ $U$  (local density approximation) method with the FLL (fully localized limit) double-counting correction [see Fig.]. The optical conductivity tensors were calculated using the `OPTIC` module [8].

structure/CIF-file	scf $k$ -mesh	$k$ -mesh for <code>OPTIC</code>
undistorted [9]	$13 \times 13 \times 5$	$28 \times 28 \times 12$
NCCDW [7]		$13 \times 9 \times 15$
CCDW [7]	$10 \times 7 \times 12$	$18 \times 12 \times 21$
<i>A</i> stacking [10]	$10 \times 10 \times 10$	$10 \times 10 \times 10$
<i>L</i> stacking [10]	$10 \times 10 \times 10$	$10 \times 10 \times 10$
<i>AL</i> stacking [10]	$8 \times 8 \times 8$	$8 \times 8 \times 8$

TABLE S1.  $k$ -point meshes used in the calculations with **Wien2k**.

Most CIF-files of the distorted structures have triclinic symmetry, in which the crystallographic *c*-axis does not align with that of the actual measured single crystal. Therefore, the optical conductivity tensors obtained from **Wien2k** must be transformed from the triclinic basis to an orthonormal basis via [11]

$$\sigma_{\text{orth}} = L \begin{pmatrix} \sigma_{xx} & \sigma_{xy} & \sigma_{xz} \\ \sigma_{yx} & \sigma_{yy} & \sigma_{yz} \\ \sigma_{zx} & \sigma_{zy} & \sigma_{zz} \end{pmatrix} L^{-1}, \quad (\text{S3})$$

with

$$L = \begin{pmatrix} a & b \cos \gamma & c \cos \beta \\ 0 & b \sin \gamma & c \frac{\cos \alpha - \cos \beta \cos \gamma}{\sin \gamma} \\ 0 & 0 & c \sqrt{1 - \cos^2 \beta - \left( \frac{\cos \alpha - \cos \beta \cos \gamma}{\sin \gamma} \right)^2} \end{pmatrix}. \quad (\text{S4})$$

Here,  $a, b, c, \alpha, \beta, \gamma$  are the triclinic lattice parameters.

## S5. ADDITIONAL COMPUTATIONAL RESULTS

DFT calculations of the undistorted structure ( $T > 550$  K) [9] reveal metallic behavior, where interband transitions are absent below  $\omega < 6000$  cm $^{-1}$  ( $\sigma_{xx}$ ) and  $\omega < 10000$  cm $^{-1}$  ( $\sigma_{zz}$ ), as presented in Fig. S3(b). The presence of lower-energy interband transitions in the experimental optical conductivity at temperatures above  $T_{CCDW} = 190$  K [see Fig. 2 in the main text] indicates a significant reconstruction of the electronic band structure in both the incommensurate CDW phase (observed above  $\sim 270$  K) and the nearly commensurate CDW (NCCDW) phase for  $190 \text{ K} < T < 270 \text{ K}$ .

Recent XRD studies suggest a domain-like star-of-David (SoD) type distortion in the NCCDW phase, whereas a uniform in-plane SoD distortion is observed in the CCDW phase. The stacking sequence in the CCDW phase was refined as  $L$  stacking and was not reported to undergo significant changes entering the NCCDW state [7]. Using the refined lattice parameters from Ref. [7], we computed the band structures for the NCCDW and CCDW phases (Fig.). In the NCCDW phase, the calculated in-plane optical conductivity reproduces the experimental results remarkably well, while the out-of-plane conductivity deviates strongly from experiment.

While the density of states at the Fermi energy is slightly reduced, the calculations do not reproduce the insulating character in the CCDW phase. While the in-plane interband response matches well with the experimental observations, the calculated out-of-plane conductivity fails to reproduce the experimental observations, overall suggesting that  $1T$ -TaS<sub>2</sub> does not adapt the  $L$  stacking neither in the NCCDW nor in the CCDW phase. Since previous studies have suggested that the gap opening in the CCDW phase could be driven by electronic correlations, i.e., a Mott insulating state, we included a Hubbard  $U = 2$  eV on the  $3d$  Ta orbitals. The resulting band structure shows almost no change (Fig. S3), consistent with other DFT studies and indicating that correlations alone cannot account for the gap opening.

Theoretical studies suggest that the gap opening in the CCDW phase is driven by interlayer stacking. Several out-of-plane structural modulations have been proposed, and we found the best agreement with the dimerized  $AL$  stacking reported in Ref. [6], as discussed in the main text. Figure S4 presents the band structures and calculated optical conductivities for different stackings using the crystal structures from Ref. [10]. Notably, an insulating state is only obtained for the  $AL$  stacking when using the modified Becke-Johnson (mBJ) exchange-correlation potential. For this configuration, the calculated optical conductivities closely match those obtained from the crystal structure in Ref. [6] [see Fig. 3 of the main text].

## S6. CALCULATION FOR DIFFRENT STACKING CONFIGURATIONS

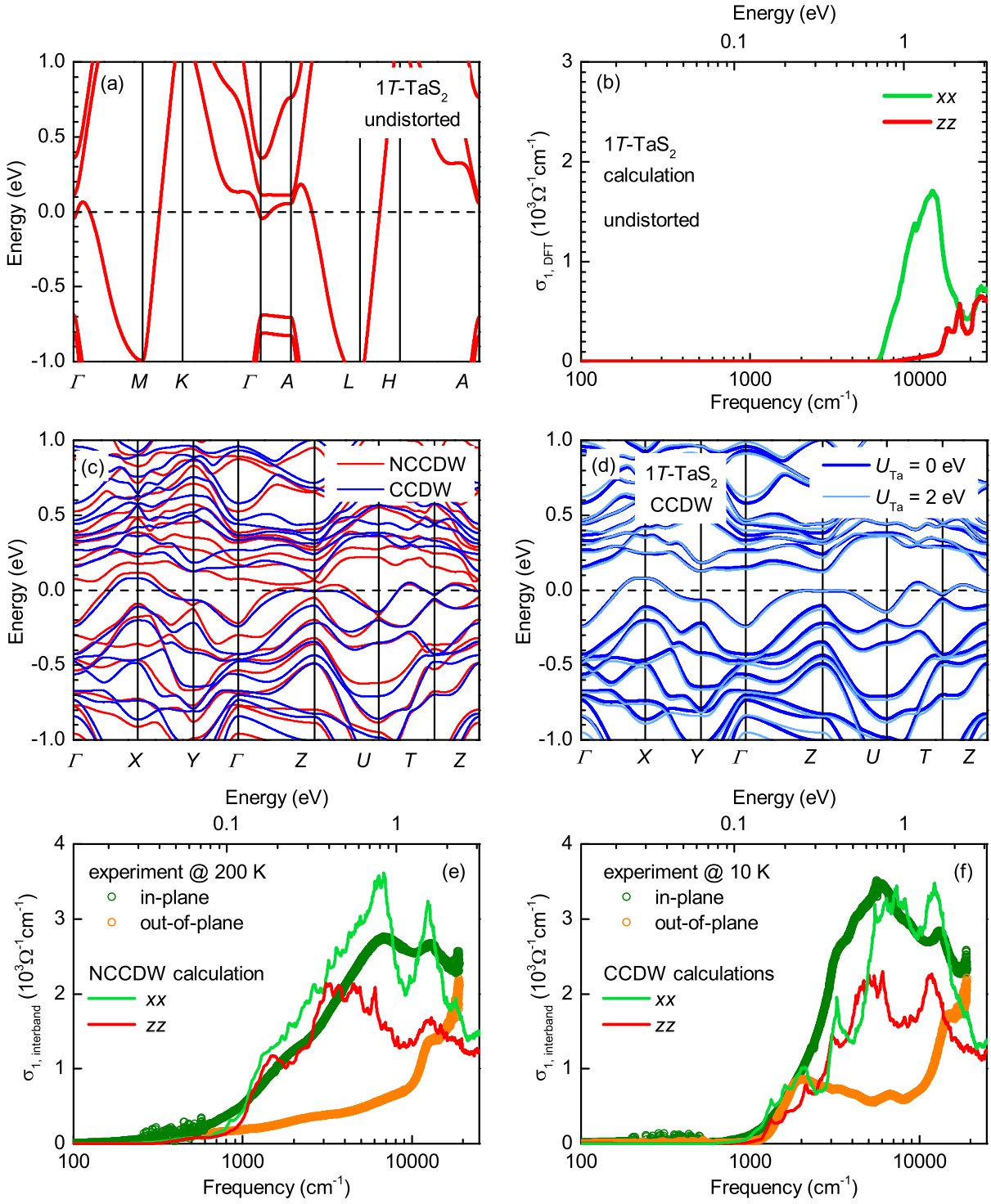


FIG. S3. (a, b) Calculated band structure and optical conductivity for undistorted phase. (c) Calculated band strucutre for NCCDW and CCDW phase. (d) Band structure for different Correlation values  $U$ . (e,f) Comparison of the measured real part of the optical conductivity,  $\sigma_1(\omega)$  for in-plane and out-of-plane, with the optical response calculated from density-functional theory for the NCCDW and CDW phase.

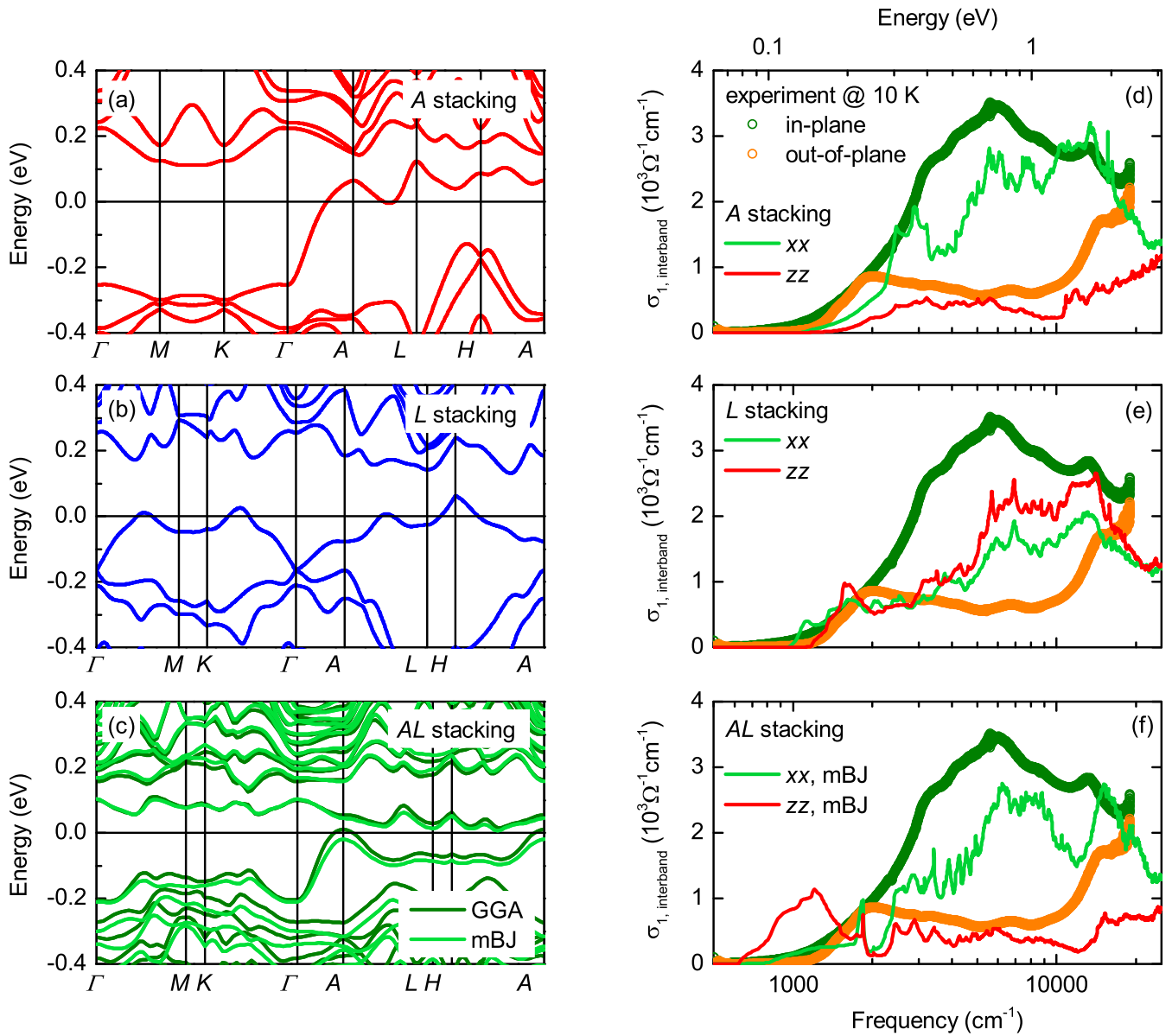


FIG. S4. (a, b, c) Calculated band structure for the low-temperature CCDW phase for A, L and AL stacking with the dashed horizontal highlights the gap at the Fermi level (d, e, f) Comparison of the measured real part of the optical conductivity,  $\sigma_1(\omega)$ , with the optical response calculated from density-functional theory for the A, L and AL-stacked commensurate CDW structure.

---

[1] P. Giannozzi, S. Baroni, N. Bonini, M. Calandra, R. Car, C. Cavazzoni, D. Ceresoli, G. L. Chiarotti, M. Cococcioni, I. Dabo, A. Dal Corso, S. de Gironcoli, S. Fabris, G. Fratesi, R. Gebauer, U. Gerstmann, C. Gougaud, A. Kokalj, M. Lazzeri, L. Martin-Samos, N. Marzari, F. Mauri, R. Mazzarello, S. Paolini, A. Pasquarello, L. Paulatto, C. Sbraccia, S. Scandolo, G. Sclauzero, A. P. Seitsonen, A. Smogunov, P. Umari, and R. M. Wentzcovitch, QUANTUM ESPRESSO: a modular and open-source software project for quantum simulations of materials, *J. Phys. Condens. Matter* **21**, 395502 (2009).

[2] P. Giannozzi, O. Andreussi, T. Brumme, O. Bunau, M. Buongiorno Nardelli, M. Calandra, R. Car, C. Cavazzoni, D. Ceresoli, M. Cococcioni, N. Colonna, I. Carnimeo, A. Dal Corso, S. de Gironcoli, P. Delugas, R. A. DiStasio, A. Ferretti, A. Floris, G. Fratesi, G. Fugallo, R. Gebauer, U. Gerstmann, F. Giustino, T. Gorni, J. Jia, M. Kawamura, H.-Y. Ko, A. Kokalj, E. Küçükbenli, M. Lazzeri, M. Marsili, N. Marzari, F. Mauri, N. L. Nguyen, H.-V. Nguyen, A. Otero-de-la

Roza, L. Paulatto, S. Poncé, D. Rocca, R. Sabatini, B. Santra, M. Schlipf, A. P. Seitsonen, A. Smogunov, I. Timrov, T. Thonhauser, P. Umari, N. Vast, X. Wu, and S. Baroni, Advanced capabilities for materials modelling with Quantum ESPRESSO, *J. Phys. Condens. Matter* **29**, 465901 (2017).

[3] P. Blaha, K. Schwarz, G. Madsen, D. Kvasnicka, J. Luitz, R. Laskowski, F. Tran, and L. Marks, WIEN2k, An Augmented Plane Wave + Local Orbitals Program for Calculating Crystal Properties (Karlheinz Schwarz, Techn. Universität Wien, Austria), 2018. ISBN 3-9501031-1-2.

[4] P. Blaha, K. Schwarz, F. Tran, R. Laskowski, G. K. H. Madsen, and L. D. Marks, WIEN2k: An APW+lo program for calculating the properties of solids, *J. Chem. Phys.* **152**, 074101 (2020).

[5] J. P. Perdew, K. Burke, and M. Ernzerhof, Generalized Gradient Approximation Made Simple, *Phys. Rev. Lett.* **77**, 3865 (1996).

[6] Y. Wang, Z. Li, X. Luo, J. Gao, Y. Han, J. Jiang, J. Tang, H. Ju, T. Li, R. Lv, S. Cui, Y. Yang, Y. Sun, J. Zhu, X. Gao, W. Lu, Z. Sun, H. Xu, Y. Xiong, and L. Cao, Dualistic insulator states in 1T-TaS<sub>2</sub> crystals, *Nat. Commun.* **15**, 3425 (2024).

[7] V. Petkov, J. E. Peralta, B. Aoun, and Y. Ren, Atomic structure and Mott nature of the insulating charge density wave phase of 1T-TaS<sub>2</sub>, *J. Phys. Condens. Matter* **34**, 345401 (2022).

[8] C. Ambrosch-Draxl and J. O. Sofo, Linear optical properties of solids within the full-potential linearized augmented planewave method, *Comput. Phys. Commun.* **175**, 1 (2006).

[9] K. Persson, [Materials Data on TaS<sub>2</sub> \(SG:164\) by Materials Project](#) (2014).

[10] T. Ritschel, H. Berger, and J. Geck, Stacking-driven gap formation in layered 1T-TaS<sub>2</sub>, *Phys. Rev. B* **98**, 195134 (2018).

[11] I.-H. Suh, Y.-S. Park, and J.-G. Kim, ORTHON: transformation from triclinic axes and atomic coordinates to orthonormal ones, *J. Appl. Crystallogr.* **33**, 994 (2000).